Effect of Magnetization on the Gel Structure and Protein Electrophoresis in Polyacrylamide Hydrogel Nanocomposites

Jeffery W. Thompson,[1] Holly A. Stretz,[1] Pedro E. Arce,[1] Hongsheng Gao,[2] Harry J. Ploehn,[2] Jibao He[3]

[1]*Tennessee Technological University, Dept. of Chemical Engineering, Cookeville, TN, 38505*
[2]*University of South Carolina, Dept. of Chemical Engineering, Columbia, South Carolina 29208*
[3]*Tulane University, Coordinated Instrumentation Facility, New Orleans, Louisiana 70161*

Received 26 August 2011; accepted 13 December 2011
DOI 10.1002/app.36660
Published online in Wiley Online Library (wileyonlinelibrary.com).

ABSTRACT: In this study, polyacrylamide nanocomposite hydrogels were formulated in combination with sodium montmorillonite (MMT) in the presence of a 2-T magnetic field. This top-down nanomanufacturing approach led to interesting changes in the internal structure of the gel and ultimately to a dramatic improvement in the ability of the composite to separate the two protein probes, ovum serum albumin and carbonic anhydrase. The morphology of the nanocomposite hydrogel was analyzed with cryogenic scanning and transmission electron microscopy, wide-angle X-ray diffraction, and small-angle scattering to determine whether morphological changes would correlate with this improved separation. As the volume fractions of MMT were well under 1% in this study (because of aqueous swelling), scattering data were dominated by the polymer structure. Significant morphological changes were noted at two length scales: (1) the hydrogel cell structure, at hundreds of nanometers, appeared to exhibit changes in the anisotropic orientation with magnetization, and (2) the polyamide structure, at tens of nanometers, exhibited decreasing pore size (small-angle X-ray scattering). The separation data correlated most closely with a reduction in pore size; however, an additional contribution to separation from local electrostatic effects from the presence of charged MMT in the cell walls could not be discounted. The change in the pore size associated with processing may have been due to the MMT presence altering the diffusion rates of the reactants during polymer formation. The method demonstrated herein could be used ultimately to separate proteins in their native state, with the potential retention of function for downstream applications, such as novel detection techniques or purification.
© 2012 Wiley Periodicals, Inc. J Appl Polym Sci 000: 000–000, 2012

Key words: clay; hydrogels; nanocomposites; orientation; proteins

INTRODUCTION

Nanocomposite hydrogels have received recent attention in the literature in terms of mechanical property enhancements. Nanocomposite hydrogels typically consist of a polyamide formed in water and a nanoparticle, such as silica,[1] clay,[2–6] or gold.[7] The array of property enhancements includes increased modulus,[8] greater strength at break and elongation,[4] variations in water uptake,[1] and changes in electronic properties,[7] as recently reviewed by Simhadri et al.[9] Hydrogels, in general, are commonly used media for the electrophoretic separation of charged particles such as DNA or proteins in clinical diagnostic applications. Nanocomposite-type hydrogels offer a number of advantages in electrophoretic applications over nonmodified hydrogels. Current sodium dodecyl sulfate polyacrylamide gel electrophoresis hydrogels typically have very poor mechanical properties,[8] poor shelf lives, and poor reproducibility of pore structure during polymerization. Nanocomposite hydrogels may offer a competitive advantage over standard hydrogel technology because of all of these properties, but little is currently understood about how the incorporation of nanoparticles into the hydrogel will affect the ultimate properties in the application of protein

Additional Supporting Information may be found in the online version of this article.

Correspondence to: H. A. Stretz (hstretz@tntech.edu).

Contract grant sponsor: National Science Foundation; contract grant numbers: IIP-0650186 (at University of South Carolina for funding that led to the characterization/purification of the MMT), DMR-0923042.

Contract grant sponsor: Scientific User Facilities Division, Office of Basic Energy Sciences, U.S. Department of Energy (for sponsoring Extended Q-range Small Angle Neutron Scattering at Oak Ridge National Laboratory).

Contract grant sponsor: U. S. Department of Energy, Office of Energy Efficiency and Renewable Energy, Industrial Technologies Program, Energy Intensive Processes Project (for sponsoring the magnetic processing research).

© 2012 Wiley Periodicals, Inc.

separation. A good dispersion of nanoparticles can eventually lead to nanochannels in the hydrogel, and single nanochannels are known to produce unique effects on biomolecular separations/transport.[10] Therefore, it is compelling that unique electrophoretic separation properties will exist for this new class of materials, which may be thought of as arrays of single nanochannels.

Matos et al.[11] showed that the inclusion of isotropic silica nanoparticles incorporated into polyacrylamide (PAAm) hydrogels altered the electrokinetic hydrodynamic mixture properties within the system. Additionally, Yu et al.[12] showed that spherical gold nanoparticles may have played a role in the separation of acidic and basic proteins in capillary electrophoresis. However, the clay platelets nanoparticles described in this article were inherently anisotropic, whereas the silica and gold in the previous case were isotropic nanoparticles. Anisotropy can uniquely affect the electrophoretic mobilities of proteins, as was recently been reported by Thompson et al.[13] for the case of gold nanorod composite hydrogels. Even when gold nanorods were randomly oriented in a PAAm hydrogel, a drastic change in the electrophoretic mobility of ovum serum albumin (OSA) protein was reported at volume fractions of less than 1% (v/v). For clay-nanoparticle-based hydrogels, some reports exist demonstrating selective DNA-type separations. Liang et al.[14] dispersed montmorillonite (MMT) into a low-molecular-weight linear polyamide-based hydrogel. The enhancement of DNA separation was attributed to an increased effective crosslink density due to the adsorption of polyamide chains on MMT platelets. Huang et al.[15] explored the effect of the introduction of multiwalled carbon nanotubes into a native gel matrix. Their study showed a change in separation, although the changes could be attributed to interactions either with the nanotubes or with the surfactant coating the nanotubes. The anisotropy of nanoparticles, however, does hold the theoretical potential to affect unique separations. Recent experimental work has shown that anisotropic morphology for a single nanochannel plays a role in separation in nanofluidic devices.[16] Therefore, an anisotropic nanophase morphology would be expected to produce a change in the electrokinetic properties of the system and, therefore, to produce unique biomolecular separations.

In this report, we describe the effects of the addition of well-dispersed, anisotropic MMT platelets to a native PAAm gel on the electrophoretic separation of proteins. The anisotropic nanoparticles were subjected to a strong magnetic field before the crosslinking of the system in an attempt to orient the platelets. Sodium MMT was selected for this study because of its susceptibility to a magnetic field in the 1–3 T range,[17] the well-characterized high aspect ratio,[18] and high areal charge density. Particle dispersion was characterized with transmission electron microscopy (TEM) and X-ray diffraction. The structure of the composite hydrogel was characterized with cryogenic scanning electron microscopy (cryo-SEM), TEM, small-angle X-ray scattering (SAXS), and small-angle neutron scattering (SANS).

EXPERIMENTAL

Materials and methods

Sodium MMT was obtained from Southern Clay Products, Gonzales, TX (Cloisite Na^+) and had a cation exchange capacity of about 91 mequiv/100 g. This MMT was dispersed and exfoliated in water on the basis of methods described previously.[18] In particular, centrifugation has been shown to remove quartz contaminants and unexfoliated platelets and to result in stock MMT suspensions containing a large percentage of dispersed single platelets. After the addition of MMT to water (1.0 g/100 mL), the suspension was sonicated for 90 min, stirred for 24 h, sonicated again for 30 min, and then centrifuged at 4000 rpm for 1 h. The resulting stock suspension was characterized by dry weight analysis, dynamic light scattering (DLS), and atomic force microscopy (AFM). (See the Supporting Information in the online version of this article for the details of this characterization.)

Acrylamide, *N*,*N*′-methylene bisacrylamide (Bis), ammonium persulfate, tetramethylethylenediamine, and high pressure liquid chromatography (HPLC) grade water water were obtained from Fisher Scientific, Suwanee GA. OSA from egg whites was obtained from Acros Organics, Suwanee GA. Carbonic anhydrase (CA) was obtained from MP Biomedicals. Trisborate ethylene diamine tetraacetic acid buffer was obtained from Ameresco. All materials were of the highest purity available and were used as received.

PAAm hydrogels were produced at 6% *T*, where %T [see eq. (1)] reflects the concentration of monomer in the solution. The hydrogels were 3% *C*, where %C [see eq. (2)] is the relationship between the crosslinker and monomer concentrations:[19]

$$T = \frac{\text{Mass}_{\text{Acrylamide}} + \text{Mass}_{\text{Bis}}}{\text{Volume}_{\text{Solution}}} \times 100(\text{g/mL}) \quad (1)$$

$$C = \frac{\text{Mass}_{\text{Bis}}}{\text{Mass}_{\text{Acrylamide}} + \text{Mass}_{\text{Bis}}} \times 100 \quad (2)$$

To prepare the composites, 3.5 g of acrylamide, 0.12 g of Bis, and variable amounts of MMT suspension were added to HPLC-grade water to ensure that the total volume of the solution was 60 mL. The MMT compositions after dilution to 60 mL for the

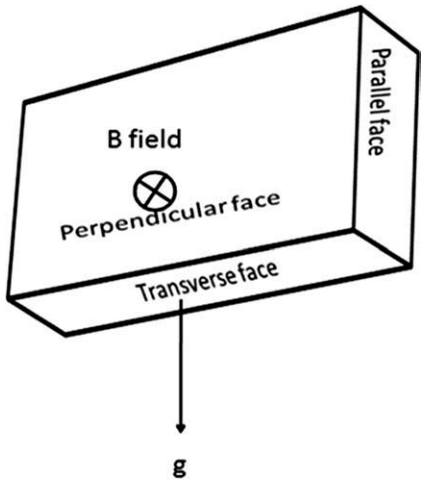

Figure 1 Schematic definition of the faces of the composite hydrogel sample, where the frame of reference for convenience is with respect to the gravity vector at the moment when electrophoresis was performed. The applied field caused the proteins to move along the direction of the gravity vector.

three samples were 0.645, 0.322, and 0.065% (w/w). The MMT content could be expressed with a variety of methods, including volume percentage (ϕ) of MMT in the entire water-swollen sample (i.e., 0.216, 0.109, and 0.021%, respectively) and weight percentage of filler with respect to the polymer (i.e., 11, 5.4, and 1.0 phr, respectively). ϕ was calculated with a value of 2.83 g/cm^3 for MMT density[20] and eq. (3), where ρ_{MMT}, ρ_{Water}, $\rho_{Acrylamide}$, and ρ_{Bis} are the densities of the respective components:

$$\phi = \frac{\text{Mass}_{MMT}/\rho_{MMT}}{\frac{\text{Mass}_{MMT}}{\rho_{MMT}} + \frac{\text{Mass}_{Water}}{\rho_{Water}} + \frac{\text{Mass}_{Acrylamide}}{\rho_{Acrylamide}} + \frac{\text{Mass}_{Bis}}{\rho_{Bis}}} \quad (3)$$

This solution was then subjected to sonication for 4 h in a Branson 5210 sonic bath Fisher Scientific, Suwanee GA. The PAAm/MMT composite hydrogels were formed by the mixture of 10 mL of the gel solution with 50 μL of ammonium persulfate (10% w/w) and 10 μL of tetramethylethylenediamine and immediately pouring of this solution into a casting apparatus. All of the samples were produced at 25°C, and they were allowed to polymerize overnight before electrophoresis.

For magnetized composites, the samples were prepared by quick placement of the glass container and hydrogel precursor contents into the center of a 5-in. bore magnet operated at 2.0 T. This exceptional apparatus was operated by Gerry Ludtka at the Oak Ridge National Laboratory High and Thermomagnetic Superconducting Magnetic Processing Facility. The applied field was perpendicular to the gravitational vector, which is our frame of reference in all future descriptions of direction (see Fig. 1). Here, the gravitational vector was the direction of gravity when the vertical electrophoresis separation was performed. Thus, the gravity vector also represented the bulk direction that the proteins traveled through the composite hydrogel. The anisotropy of the casting apparatus offered a convenient method to track the magnetic orientation direction during subsequent handling/processing. The magnetic field strength was uniform (±1%) over the area in which the composite hydrogel was exposed. Samples were removed from the bore after approximately 40 min and were observed to be solidified. At that time, we assumed that the nanoparticles were effectively frozen into place and could not relax back into a random arrangement because of the constraint presented by the crosslinked gel solids around them. The samples were allowed to polymerize overnight before electrophoresis.

No postprocessing of the gels (control, filled, or magnetized), such as swelling or rinsing, was performed because such procedures could have altered the nanoparticle structure induced by the magnet.

TESTING AND CHARACTERIZATION

TEM

Filled PAAm/MMT samples were prepared for microscopy by the polymerization of 2 μL of a

TABLE I
Digital Image Analysis Results and Hydrogel Cell Diameters

Sample	View orientation	n	Number-average cell size (nm)[a]	Weighted-average cell size (nm)[a]	Ratio of the large/small feature size (anisotropy)	Direction of anisotropy[b]
Control	Transverse	315	477	526		
Control	Parallel	240	591	637	591/477 = 1.24	P→T
Magnetized	Transverse	451	400	432		
Magnetized	Parallel	436	278	296	400/278 = 1.44	T→P
Random	Transverse	264	587	632		
Random	Parallel	98	227	238	587/227 = 2.58	T→P

P, parallel; T, transverse.
[a] The standard deviations were approximately 50–150 nm.
[b] The directions of anisotropy are defined with respect to the Figure 1 orientations.

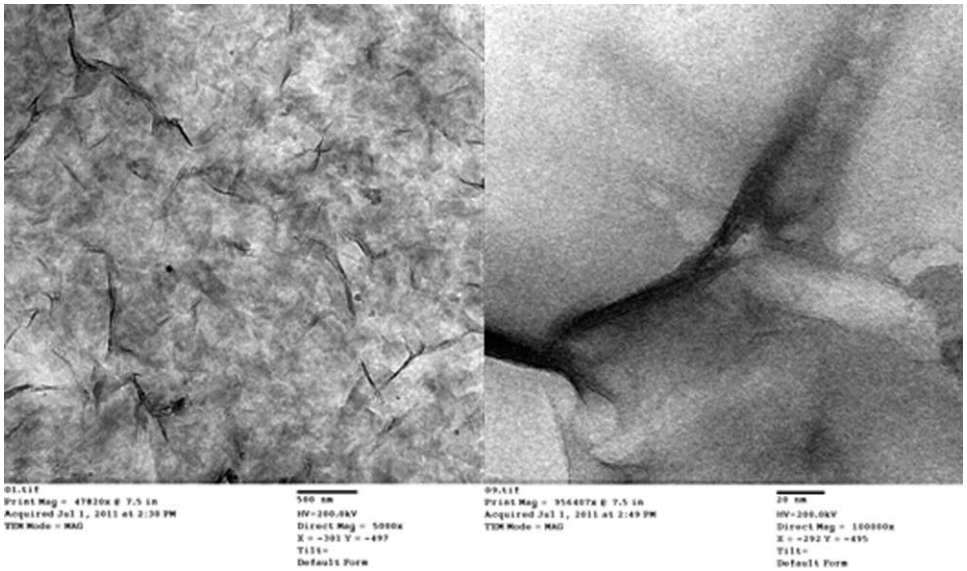

Figure 2 TEM photomicrographs of MMT in the filled hydrogel polymerized on the TEM grid ($\phi_{MMT} = 0.22\%$).

hydrogel solution onto the surface of a carbon-coated, 300-mesh Cu TEM grid. Photomicrographs were produced at Tulane with a JEOL JEM-2010 instrument, Peabody, MA operating at 100 kV.

Wide-angle X-ray diffraction

Wide-angle X-ray diffraction was performed on filled PAAm/MMT composite gels to obtain information about the dispersion of the clays. Typically, sodium MMT shows an X-ray peak at a $2\theta = 6.11^\circ$.[21] Scans were taken on a Rigaku Ultima IV diffractometer The Woodlands, TX with Cu Kα radiation with rotation of the samples at 20 rpm. To get sufficient counting statistics, each sample was scanned for approximately 2 h.

SAXS and SANS

Small-angle scattering was employed to obtain some information about the gel microstructure (e.g., pore diameters) and potential orientation of the MMT. For small angle X-ray scattering (SAXS), the samples were mounted such that the X-ray beam passed through the perpendicular face (see Fig. 1). Sample scans were taken on the previously described Rigaku Ultima IV device with a small-angle scattering attachment in transmission mode at a fixed sample angle of 1.5000°. In this mode, the detector was then scanned from 0.1 to 8.0°. The scanning speed was 0.012°/min; this led to a scan time of about 11 h for each sample to obtain sufficient counting statistics.

Small angle neutron scattering (SANS) was performed on the control and randomly oriented composite gels on a beamline BL6 extended Q-range small angle neutron scattering (EQ-SANS) at the Spallation Neutron Source, Oak Ridge National Laboratory Oak Ridge, TN, in collaboration with Dazhi Liu. The incident neutron beam penetrated the perpendicular face (see Fig. 1).

Cryo-SEM

Different samples were cut to expose two of the faces, the parallel and transverse faces, as defined in Figure 1. We then froze the samples by dipping the mounting/sample in liquid nitrogen (with oxygen removal before dipping to prevent convection) then mounted to a Hitachi S-4800 field emission scanning electron microscope with a cryogenic stage attachment. After mounting, the samples were freeze-fractured with a 130, 95, 130-K temperature cycling process. The water was removed by sublimation to eliminate the possibility of surface-tension-derived artifacts associated with a traditional drying process. The representative nature of this sample preparation procedure for hydrogel morphology has been discussed elsewhere.[22–27] Images were also produced for the third face, the perpendicular face, but the hydrogel was too thin to be mounted in a manner consistent with the fracturing procedure described previously, and these images were not of a quality necessary for subsequent analysis. Multiple images for the other two faces were produced in random positions and at various magnifications, and these were analyzed digitally to produce statistics on the feature dimensions with Adobe Photoshop. The features (e.g., cells) were individually measured in Photoshop along both a long and short axis, and an average of the two values was counted for analysis. Only the cells in the fracture plane were used. The number of features (n) measured are shown in Table I. Two types of averages are presented, a number average and a weighted average. These values were calculated with the following

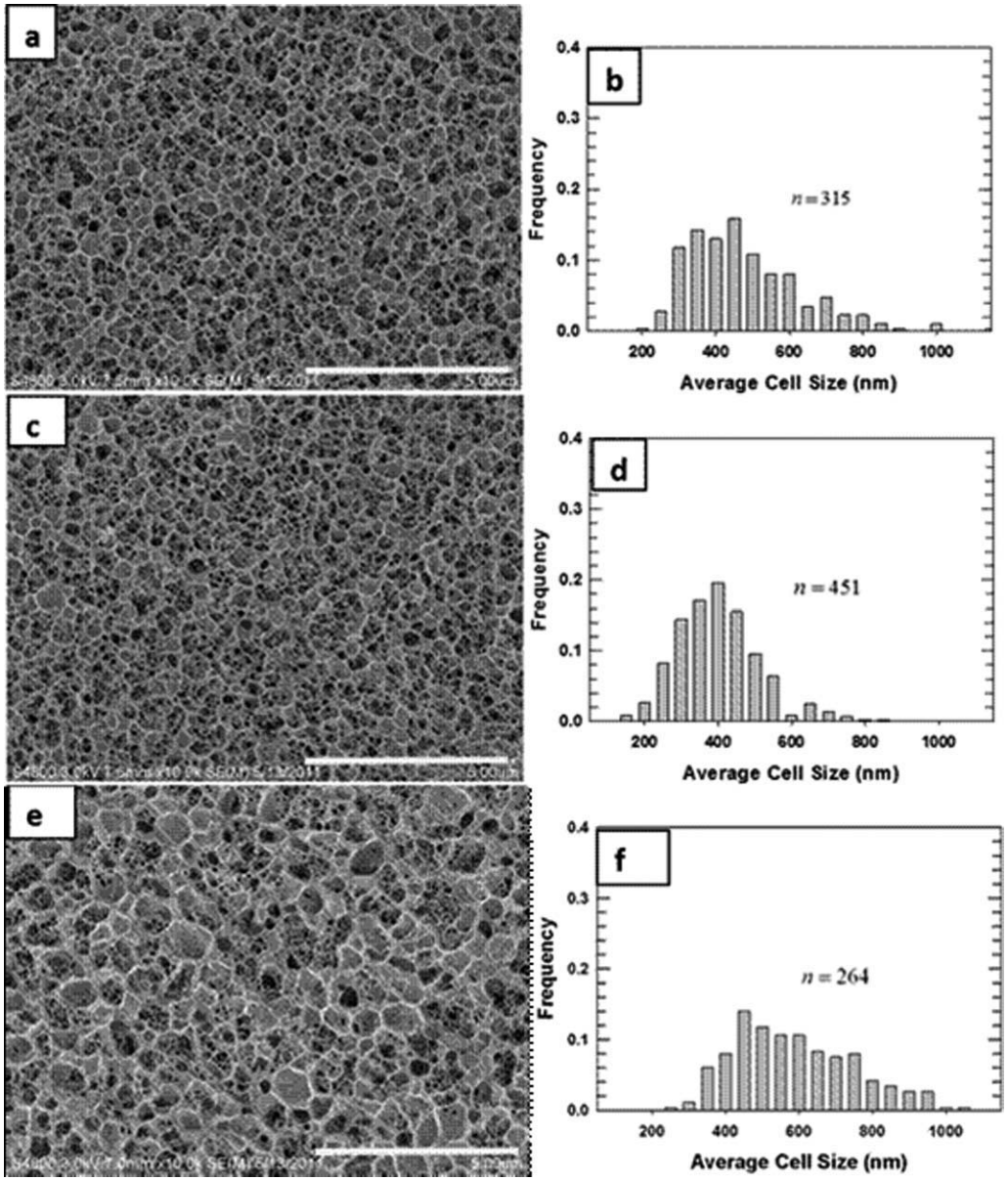

Figure 3 Representative photomicrographs (with cryo-SEM) of the transverse-face fracture surfaces for the (a,b) control gel, (c,d) magnetized-filled gel, and (e,f) filled gel. A histogram resulting from the digital image analysis of the cell diameter is presented next to each corresponding image. The larger features indicate cells, and the holes in the walls of the cells indicate pores. All of the scale bars represent 5 μm ($\phi_{MMT} = 0.22\%$).

equations, where n_i is the number of particles with average diameter d_i:

$$\text{Number average} = \frac{\sum_i n_i d_i}{\sum_i n_i} \quad (4)$$

$$\text{Weighted average} = \frac{\sum_i n_i d_i^2}{\sum_i n_i d_i} \quad (5)$$

Electrophoretic testing

All hydrogels were tested for electrophoretic separation characteristics. The gels were cast at 10 cm × 10 cm × 0.8 mm and were immersed in a trisborate ethylene diamine tetraacetic acid buffer at pH 8.0. Dansyl chloride labeled OSA and dansyl chloride labeled CA (10 μL with a 1 mg/mL concentration) were loaded into the gel lanes. Gel electrophoresis was performed at constant voltage (6.67 V/cm) for a period of 45 min with a Fisher FB1000 power supply Fisher Scientific, Suwanee, GA. (Note that the voltage not the current was specifically controlled.) After electrophoresis, the gels were placed under a UV lamp–illuminator apparatus home assembled, Porter's Camera, Cedar Rapids, IA to measure the protein band position and to determine the electrophoretic velocities. For the case of the filled hydrogels,

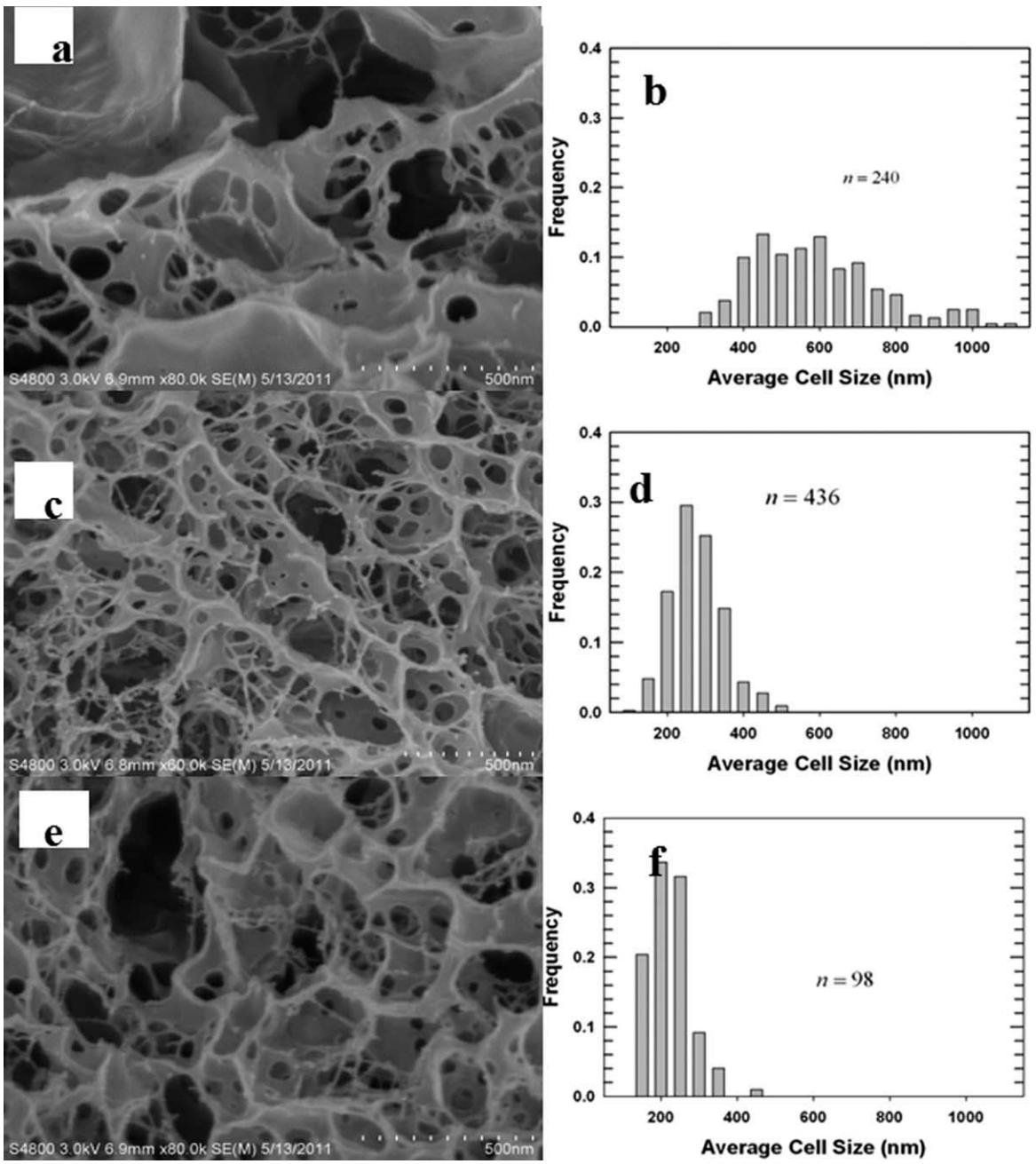

Figure 4 Representative photomicrographs (with cryo-SEM) of the parallel-face fracture surfaces for the (a,b) control gel, (c,d) magnetized-filled gel, and (e,f) filled gel. A histogram resulting from the digital image analysis of the cell diameter is presented next to each corresponding image. Larger features indicate cells, and the holes in the walls of the cells indicate pores. All of the scale bars represent 500 nm ($\phi_{MMT} = 0.22\%$).

five replicates were tested. For the case of the magnetized-filled hydrogels, only two replicates were tested because of limited user time on the Oak Ridge National Laboratory magnet.

RESULTS

To gain valuable insight in terms of the structure–property relationships, the novel composite hydrogel material morphology was characterized rigorously. This involved three types of samples. The crosslinked hydrogel control had no nanoparticles. The nanocomposite hydrogel formed in the presence of water-dispersed sodium MMT is referred to as *filled*, and the orientation of the MMT was not intentionally manipulated. The nanocomposite hydrogels formed in the presence of a uniform 2-T magnetic field are termed *magnetized-filled*. In the latter case, we assumed that any orientation occurred faster than the polymer crosslinking process, a reasonable assumption given previous reports by Koerner

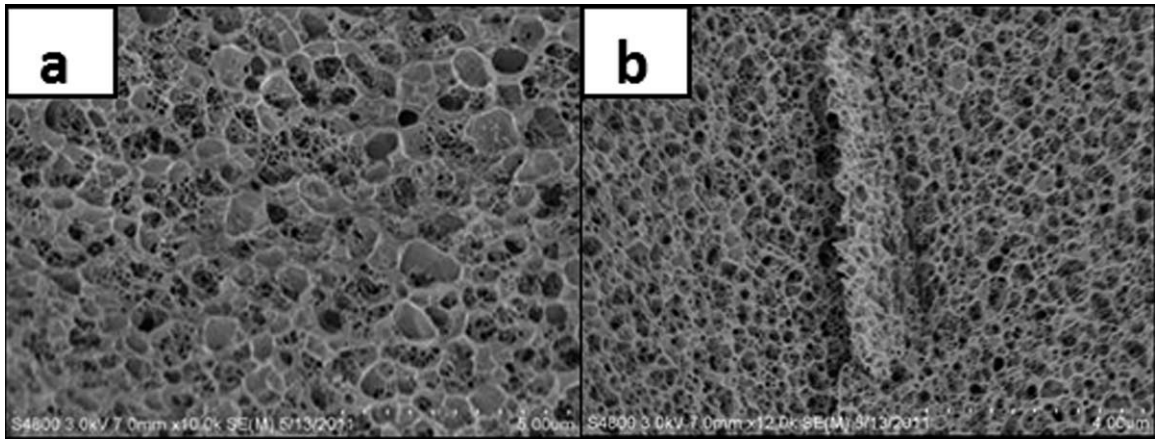

Figure 5 Representative photomicrographs (with cryo-SEM) of the parallel-face fracture surfaces for the (a) control gel (scale bar = 5 μm) and (b) magnetized-filled gel (scale bar = 4 μm). The holes in the walls of the cells indicate the pores. These parallel-face images are not all in the same scale as in Figure 3 ($\phi_{MMT} = 0.22\%$).

et al.[17] on the orientation of MMT in epoxies. *T* (6%) and *C* (3%) were the same for all three types of samples. A thorough discussion of the hydrogel morphology obtained under these three processing conditions follows, and subsequently, a discussion is presented of the electrophoresis results for the two model proteins used as probes: OSA and CA. The morphology and electrophoresis are then compared.

Nanoparticle characterization

The MMT solution was characterized by both AFM and DLS according to procedures that were previously published.[18] AFM showed an average particle size of 201 nm, an average particle thickness of 1.3 nm, and an average aspect ratio of 159. DLS showed an effective hydrodynamic diameter of 219 nm; this was in reasonable agreement with the size from AFM. On the basis of the AFM results, about 83% of the MMT particles in the suspension were pristine single platelets, and 98% were either singlets or doublets (see the Supporting Information for more details).

Figure 2 presents TEM photomicrographs of the MMT particles in the filled hydrogel. The MMT particles were not as well exfoliated as the original well-characterized Na-MMT water suspension (previously discussed); however, they were still well dispersed.

Structure of the hydrogels

To discuss the hydrogel structure, we refer again to Figure 1 as the frame of reference for viewing the hydrogels along the various directions: a transverse face, a parallel face, and a perpendicular face. The cryo-SEM samples were prepared to produce images along these three faces with great care to preserve the submicrometer structure. *In situ* cryogenic techniques were used for sample handling, and the images were of a planar fractured surface. Representative photomicrographs of the transverse face of the three formulations are compared in Figure 3. Representative photomicrographs of the parallel face of the materials are compared Figure 4. The magnifications from Figures 3 and 4 do not match, so additional images are presented in Figure 5, with a view along the parallel face to provide a more complete comparison. Corresponding histograms of the digital image analysis results are also presented in Figures 3 and 4 and are discussed. Statistical information about these feature dimensions are listed in Table I. Although images were obtained along the perpendicular face, the fracture techniques did not produce representative features, and thus, these images are not discussed.

Qualitatively, we initially noted when viewing Figures 3 and 4 that features in a single photomicrograph existed at multiple scales, and a convention needed to be adopted to describe the various features. A materials science approach is used to aid the discussion. The larger features in these images resemble the cells in polymer foams and, thus, are termed *cells*. The walls or membranes forming these cells were sometimes closed and sometimes exhibited small holes. The holes might be expected to be the most resistive element associated with the mass transport of solutes, at least in terms of molecular sieving. The holes in the walls are termed *pores*. The spaces between crosslinks, which were too small to be seen in these images, are termed *free volume*. Stellwagen[28] recently published a review on the structure/property relationships in the electrophoresis of biomacromolecules that discusses the importance to mass transport of the two distinct feature sizes. Although terminology from the materials science

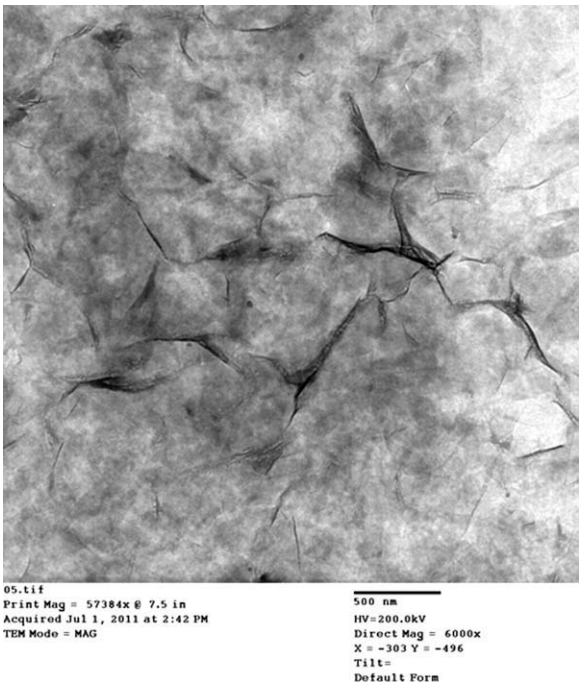

Figure 6 TEM image of the PAAm/MMT hydrogel (filled hydrogel). The MMT platelets bent around the individual cells in the hydrogel but did not completely enclose any one cell. The cell walls cannot be seen in these images because they were composed of carbon-based polymer and did not scatter the beam as effectively as the aluminosilicate MMT did ($\phi_{MMT} = 0.22\%$).

perspective versus the electrophoresis perspective may not overlap, the presence of the two feature sizes that Stellwagen discusses certainly matches these observations.[28] Another general issue to note in these scanning electron microscopy (SEM) images is the absence of any feature easily attributed to the presence of MMT nanoparticles, and this is discussed later.

One clear observation in a comparison of the number-average cell diameters, as listed in Table I, is that all of the features exhibited some anisotropy. The control PAAm hydrogel had a smaller average cell diameter when viewed along the transverse direction (477 nm) than when viewed along the parallel direction (591 nm). The ratio of these values (larger/smaller) was 1.24. Similarly, the magnetized-filled hydrogel had a smaller cell diameter of 278 nm and a larger diameter of 400 nm; this yielded an apparent anisotropy ratio of 1.44. The differences in these ratios may not have been significant, but what was very different about the two materials was the direction of this anisotropy. In the case of the control hydrogel, the largest features were seen along the parallel direction, and the opposite was true for the magnetized-filled hydrogel. One possible explanation for the anisotropy in the control was that the presence of the glass boundary affected cell formation and led to constrained cell dimensions in one direction. This result was consistent with reports by Gemeinhart et al.,[29] in which the type of glass used (hydrophobicity or hydrophilicity of the glass coating) influenced the hydrogel cell structure and led to pseudo-cylindrical cell geometries. In the case of the composite hydrogel cells, we hypothesized that the MMT had, instead, templated the formation of the cells during polymerization. The MMT platelets are thought to be reinforcing agents within the cell walls in these images [Figs. 3(c) and 4(c)], with individual platelets collecting at this interface and bending with the curvature of the cell wall, although never completely enveloping a cell. (This bending or conforming at an interface has been observed by many others, including by Stretz et al.[30] for multiphase poly(acrylonitrile–butadiene–styrene)/MMT nanocomposites). The MMT platelets were not distinguishable in the SEM images here because they were too thin to resolve and because they appeared white; this was hidden by the bright white edges of the cell walls. Evidence supporting the presence of MMT dispersed throughout the gel is shown in Figure 6. This TEM photomicrograph of the composite hydrogel on a TEM grid shows the MMT platelets bending around some invisible domain (the carbon-based polymeric cell walls cannot be seen in a TEM image) but never completely enclosing the domain. Because the MMT platelets were present in the cell walls as the walls were forming, they could affect the directionality of the forming wall. Nie et al.[31] concluded, for instance, that oligomeric PAAm attaches to the MMT initially, and this reduces the mobility of growing chains, which is consistent with the MMT acting as a template for cell wall growth. The combination of a reinforcing wall template (MMT) and orientation of the MMT in the magnetic field could have been responsible for the change in the directionality of the cells. Table I also shows that the composite hydrogels that were not exposed to a magnetic field exhibited the same reversed directionality of the cells when compared to the control hydrogel; however, the cells were inexplicably much larger when viewed along the transverse direction (587 nm) in this less controlled case. These larger dimensions may not be desirable during electrophoresis, as discussed later.

SAXS and SANS

Originally, the MMT in the magnetized samples was expected to be oriented, as seen by Koerner et al.,[17] for epoxy/MMT composites. Therefore, both SAXS and SANS were performed in hopes of characterizing the bulk degree of platelet orientation. The

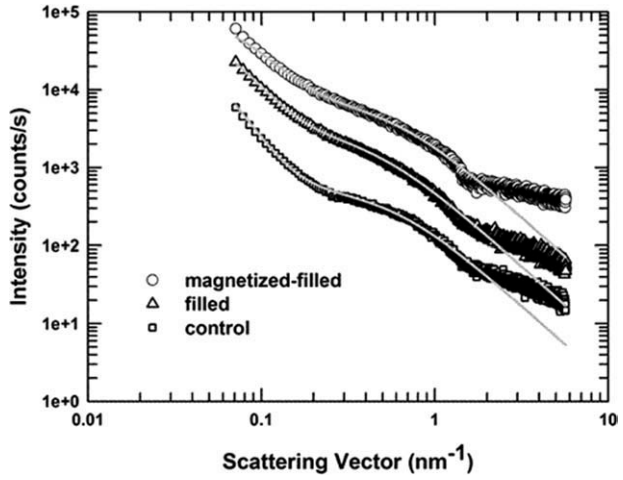

Figure 7 I values from the SAXS measurements (symbols) for the control PAAm hydrogel, filled hydrogel, and magnetized-filled hydrogel. The solid curves are the theoretical fits based on the model described in the text. The data points and theoretical curve for the filled and magnetized-filled hydrogels were shifted up by factors of 2 and 10, respectively, for clarity ($\phi_{MMT} = 0.22\%$) for the filled and magnetized-filled samples.

samples analyzed were at the highest MMT concentration corresponding to $\phi = 0.22\%$ (v/v). Other ways to express this filler concentration for the same sample would be weight percent $w = 0.6\%$ (w/w) or 11 phr.

Data analysis

The scattered intensity (I) as a function of the momentum transfer (q) from SAXS and SANS measurements were fit with a theoretical expression suitable for crosslinked hydrogels, including PAAm[32] and other polymers[33–37]:

$$I(q) = \frac{I_{DB}}{\left(1 + \Xi^2 q^2\right)^2} + \frac{I_L}{1 + \xi^2 q^2} \quad (6)$$

The first term is the Debye–Bueche expression[38] for scattering due to long-range density fluctuations [correlation length associated with the long-range density (Ξ)], described in terms of a two-density random medium with a sharp interface.[39] The second term is a Lorentzian function for scattering from semidilute polymer solutions with the correlation length associated with the short-range density (ξ). The parameters values were established in the way suggested by Koberstein et al.[38] First, with Zimm plots (I^{-1} versus q^2), linear fits of the data in the range $0.1\ \text{nm}^{-2} < q^2 < 1.2\ \text{nm}^{-2}$ were used to determine values of the Lorentzian intensity (I_L) and ξ. The excess scattering (I_{ex}) for the range $q^2 < 0.1\ \text{nm}^{-2}$ was computed as

$$I_{ex}(q) = I(q) - \frac{I_L}{1 + \xi^2 q^2} \quad (7)$$

Finally, with Debye–Bueche plots ($I_{ex}^{-1/2}$ versus q^2), linear fits of the data in the range $q^2 < 0.04\ \text{nm}^{-2}$ were used to determine values of the Debye–Bueche intensity (I_{DB}) and Ξ.

Results

Figure 7 shows the scattered intensity [$I(q)$] values for various hydrogels from the SAXS measurements. Model predictions appear overlaid here as the thin lines behind the scatter data. In general, the shapes of the $I(q)$ curves for the PAAm/MMT hydrogels were similar to that of the control PAAm hydrogel. This suggested that scattering from the PAAm gel structure dominated in all of the samples. At larger scattering angles ($q > 1.5\ \text{nm}^{-1}$), $I(q)$ decreased approximately as q^{-1}; this could be seen more clearly in Kratky plots [$q^2 I(q)$ vs q (see the Supporting Information, plots S4–S6)], which were linear for $q > 1.5\ \text{nm}^{-1}$. This scattering pattern indicated a rodlike structure and is expected for polymers at length scales smaller than the chain persistence length.[40] The transition to I–q^{-1} behavior occurred at about $q = 1.5\ \text{nm}^{-1}$ and corresponded to a persistence length ($L_p^0 = 1/q$) of about 0.66 nm or a Kuhn (statistical segment) length of about 1.33 nm. This agreed closely with the Kuhn lengths previously reported for PAAm and which ranged from 1.0 to 1.7 nm.[41–43] This result, observed for the PAAm/MMT composites and the control PAAm, further supported the conclusion that the SAXS pattern primarily manifested the structure of the PAAm gel. The presence of MMT in the composites seemed to have little effect on the SAXS pattern, presumably because of its low weight loading (0.6 wt %).

For $q < 1.5\ \text{nm}^{-1}$, eq. (6) fit the scattering data well. Table II shows the parameter values. The good fit of the Lorentzian term at intermediate q values (~ 0.3–$1.5\ \text{nm}^{-1}$) indicated scattering from a semidilute polymer solution with characteristic ξ between entanglement points. The value of ξ for the PAAm gel (1.8 nm) agreed with values found in a previous work.[32] The value of ξ for the magnetized-filled hydrogel was similar, but that for the filled PAAm/MMT gel was higher (2.3 nm). We do not know if

TABLE II
Model Parameters Obtained from the SAXS Data with eq. (6)

	I_L	ξ (nm)	I_{DB}	Ξ (nm)
Control hydrogel	531	1.8	89,100	24.0
Filled hydrogel	1460	2.3	45,000	15.2
Magnetized-filled hydrogel	726	1.8	9,600	10.4

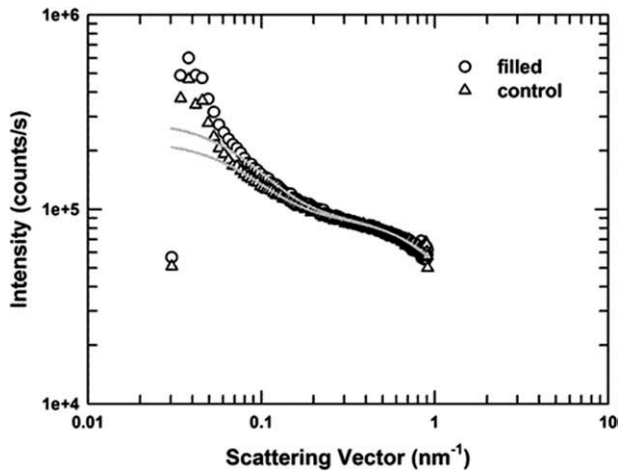

Figure 8 I values from the SANS measurements (symbols) for the control PAAm and filled hydrogels. The solid curves are the theoretical fits based on the model described in the text ($\phi_{MMT} = 0.22\%$) for the filled and magnetized-filled samples.

this observation was significant. The Debye–Bueche term fit the SAXS data well at lower q values. The quantity Ξ represents the characteristic length scale associated with long-range density fluctuations created by crosslinks in the polymer network. The control PAAm gel had a value of Ξ of 24.0 nm, which was in reasonable agreement with that found previously.[32] However, we find a 37% smaller value of Ξ for the filled PAAm/MMT hydrogel (15.2 nm). For the magnetized-filled hydrogel, Ξ was 34% smaller than that of the random hydrogel and 58% smaller than the control hydrogel. These observations indicated that the presence of MMT had a discernible effect on the larger scale domain structure associated with the crosslinked PAAm network.

Figure 8 shows $I(q)$ for the control and filled PAAm/MMT hydrogels from SANS measurements, with model predictions based on eq. (6) overlaid as solid curves (fit parameter values given in Table III). The shapes of the $I(q)$ curves for the control and filled PAAm/MMT hydrogels were very similar. Equation (6) fit the SANS data well for $q > 0.07$ nm^{-1}. However, the correlation lengths were smaller than those obtained from the SAXS data, and there was no difference between the control PAAm and filled PAAm/MMT gels ($\xi = 0.8$ nm and $\Xi = 8.7$ nm for both gels). This may have been due to the low contrast difference between the gel and H_2O in SANS, which resulted in a poorer discrimination of the gel structure than seen in the SAXS results. Also, both SANS patterns showed a peak at about $q = 0.04$ nm^{-1} located below the q range probed by SAXS. These peaks suggested a microstructure with a characteristic length scale of $2\pi/q \approx 150$ nm. We speculated that this length scale may have been associated with the cell size observed in the cryo-SEM images. This point should be addressed in greater depth with SANS with contrast variation (via the D_2O/H_2O ratio).

Discussion of characterization

At this point, we can only speculate as to the mechanism by which MMT influenced the topology of the forming crosslinked PAAm network. The presence of MMT and the process of magnetization in the precured solution affected the diffusion of acrylamide and bisacrylamide during the curing process and, thus, the network topology of the gel. In the absence of platelets, the reactant diffusion was unimpeded; the bisacrylamide could react and form larger knots that were smaller in number and relatively far apart ($\Xi = 24.0$ nm). In the presence of randomly oriented MMT platelets, bisacrylamide diffusion was hindered; this resulted in a larger number of somewhat smaller knots that were, consequently, closer together ($\Xi = 15.4$ nm). If the magnetic field aligned the platelets during an early polymerization stage, diffusion was hindered even more, as predicted by barrier models.[44–47] This further increased the number of knots and reduced their size and spacing ($\Xi = 10.2$ nm). Two aspects of this hypothesis will need to be tested. First, we may need to obtain direct evidence that the magnetic field aligns MMT platelets in the precured acrylamide/bisacrylamide solutions; the work of Koerner et al.[17] strongly suggests alignment under our conditions, but verification during the cure would be desirable. Second, further structural studies involving the systematic variation of bisacrylamide concentration in the presence of MMT would be helpful. The effect of the crosslinker concentration on the PAAm gel structure seems to be well understood.[48–50]

Electrophoretic testing

In Figure 9, the effect of increasing the nanoparticle content (in the absence of magnetization) on the electrophoretic mobilities are presented for two proteins: CA [molecular weight (MW) = 28,900, pI = 5.9[51]] and OSA (MW = 45,000, pI = 4.6[52]). Note that the mobilities presented in Figure 9 were normalized by the corresponding mobility for the control.

TABLE III
Model Parameters Obtained from the SANS Data with eq. (6)

	I_L	ξ (nm)	I_{DB}	Ξ (nm)
Control hydrogel	91,600	0.84	134,000	8.7
Filled hydrogel	92,600	0.87	192,500	8.7

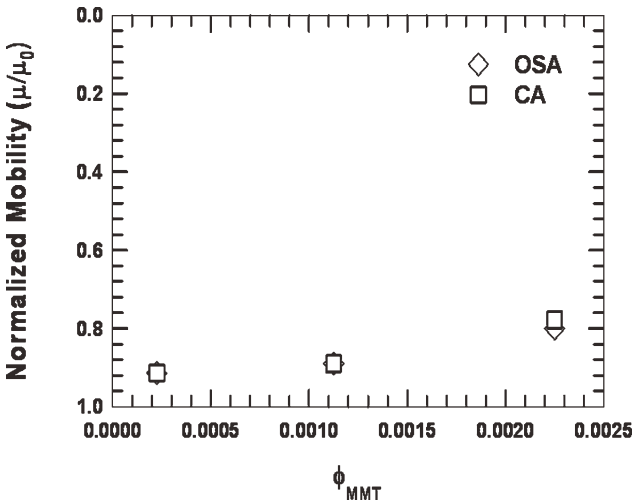

Figure 9 Electrophoretic mobilities μ versus mobility in the control hydrogel μ_0 measured in the nanocomposite filled gels for the two proteins OSA and CA. ϕ is the volume percent montmorillonite (MMT) in the composite

Increasing filler content lowered the mobility of both proteins. This result was consistent with a tortuous path effect, which our previous work demonstrated was one appropriate model for an OSA protein probe at the same electrical field moving through a composite hydrogel of PAAm/gold nanoparticles.[13] However, some separation of the two proteins was achieved at the highest loading of MMT nanoparticles. Producing hydrogels with greater MMT content was impractical because the MMT suspension was provided at a certain concentration, and the processing of the suspension (e.g., by centrifugation) to concentrate it could have resulted in changes in the excellent dispersion of nanoparticles.

As shown in Figure 10, magnetizing the MMT nanoparticles during gel formation led to a very different electrophoretic result. Increasing the loading of magnetized nanoparticles improved separation in all of the compositions. (Note that the analysis was replicated with hydrogels magnetized at a separate time, and duplicate results were plotted but could not be resolved on this scale. Please see the Supporting Information, Fig. S7, for an overlay of the chromatographic-type peaks indicating excellent reproducibility.) OSA and CA would be otherwise difficult to separate (they were inseparable in the control gel) because molecular sieving is not sensitive enough in general to differentiate these MWs. Something intrinsic to the addition of MMT in connection with magnetization produced a unique separation. An important feature of this separation was that the proteins did not need to be denatured (e.g., by sodium dodecyl sulfate in standard sodium dodecyl sulfate polyacrylamide gel electrophoresis separations) to achieve separation. The proteins could retain their activity for later downstream applications such as novel detectors or purification.

In terms of the structure/property relationships, four models could be invoked to explain these data. The first was previously discussed, that is, the tortuous path effect. Here, we would have expected the protein velocity to slow down because the impermeable high-aspect-ratio MMT particles presented a tortuous path. For magnetized-filled PAAm/MMT, the proteins moved more slowly on average than they did in the filled PAAm/MMT. Both composite hydrogels had the same concentration of MMT; therefore, tortuous path theory alone did not predict all aspects of protein velocity. The other three models we discuss include (1) that cell size affected mobility, specifically that smaller cells along the direction of the protein movement caused the protein to encounter more cells; (2) that wall charge affected the mobility and that wall charge was a function of the presence of the embedded MMT; and (3) that crosslink or pore size affected the mobility and presence of MMT during gelation and led to changes in the crosslinks or pore structure. Consider that the size of the cells might have affected the mobilities. Along the cryo-SEM parallel view, the control exhibited 591 nm diameter cells, whereas the nanocomposite exhibited 278 nm diameter cells. This meant that the proteins traveled through about 50% more cells in the nanocomposite versus the control. More cells could have meant more interactions and could have led to separation. This effect should have been true for both random and magnetized nanocomposite gels, and indeed, some evidence of improved separation could be seen for both but not to the same extent. This hypothesis does not explain all of the differences observed in the composition effect nor why CA moved selectively faster than OSA. Therefore, the effect of the cell size was not seen to

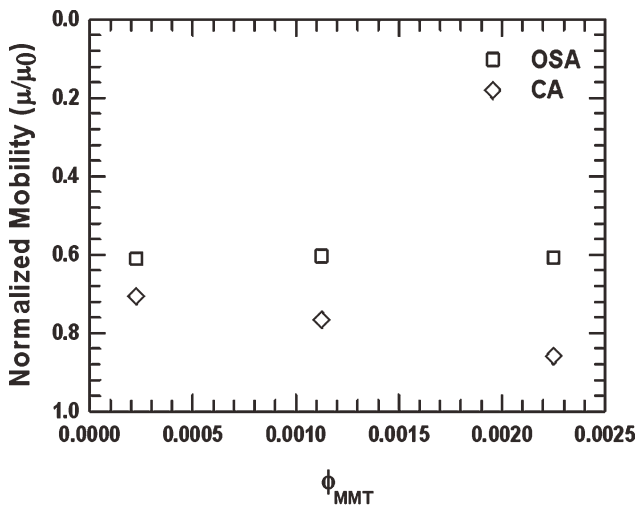

Figure 10 Electrophoretic mobilities μ versus mobility in the control hydrogel μ_0 measured in the nanocomposite magnetized-filled gels for the two proteins OSA and CA. ϕ is the volume percent montmorillonite (MMT) in the composite.

contribute to this particular separation. (Note that the features we designated as cells, seen in cryo-SEM, were not the same features as molecular-scale crosslinks, which SAXS measured.)

We consider now that the walls of the nanocomposites might have had a different charge. A consequence of increasing the number of cells encountered by the protein in the filled hydrogels would have been increased wall exposure. As the MMT particles had a surface charge density of about 91 mequiv/100 g, electrostatic contributions could have influenced separation. The OSA may have had an affinity or repulsion for a charged MMT wall. OSA would have been expected to have a higher charge density at the buffer pH = 8 than CA. (The pI for OSA was lower.) CA traveled faster in the composite hydrogels versus OSA (as was most evident in the magnetized hydrogel), and this was consistent with more electrostatic repulsion for CA. Also, if the charged walls of the cells altered the electroosmotic flow characteristics, separation may have resulted.[53] In conclusion, the charged wall scenario could have explained the differences in the mobilities of CA and OSA but not why that separation was more pronounced in the magnetized-filled gels versus the filled gels.

Finally, we considered that the pores and crosslinks in the gels changed during polymerization. The SAXS data supported this hypothesis. The Debye–Bueche characteristic length (Ξ) in Table II decreased in the following order: Control > Filled > Magnetized-filled. This order correlated with the degree of electrophoretic separation noted for CA versus OSA. In other words, the control Ξ was the largest value, and this correlated with no separation. The random Ξ was intermediate in size, and separation was barely noted, only at the highest MMT concentration. The magnetized Ξ was the smallest value, and this correlated with the most improved separation. In conclusion, the small pore/crosslink scenario could explain the differences in the mobilities of CA and OSA and could also explain why the magnetized-filled hydrogel produced better separations than the filled hydrogel.

The review by Stellwagen[28] indicated that molecular sieving alone would not be expected to produce optimized separations for proteins; thus, a combination of effects was the most likely explanation for separation in this study.

CONCLUSIONS

Anisotropic MMT nanodiscs were successfully incorporated into a PAAm matrix in two formats: the MMT particles were randomly mixed (filled) in one, and in the other, the whole system was exposed to approximately 2 T of magnetic field during polymerization (magnetized-filled hydrogel). Electrophoresis (separation of CA and OSA) led to reduced protein mobility in both the composites, but for the magnetized-filled gels, good separation of the two proteins occurred for all compositions of MMT tested. For the filled gels, separation of the proteins occurred only at the highest filler concentration studied. The structures of the three hydrogels were characterized to correlate with the structure with this novel separation. Cryo-SEM studies showed that cells for the magnetized-filled and filled gels were much smaller along the parallel direction than in the case of the control. The parallel direction was the direction in which the proteins moved during electrophoresis. In addition, SAXS and SANS data were interpreted in terms of fits to the Lorentzian and Debye–Bueche models. Ξ showed decreasing pore diameters of 24, 15, and 10 nm for the control, filled, and magnetized-filled gels, respectively. This order correlated closely with the degree of electrophoretic separation noted in the three hydrogels for the proteins. For the magnetized-filled hydrogel, Ξ was 34% smaller than that of the random hydrogel and 58% smaller than the control hydrogel. These observations indicated that the presence of MMT had a discernable effect on the larger scale domain structure associated with the crosslinked PAAm network, potentially because of diffusion constraints for the reactants during the polymerization step. Much of the improved separation was likely due to smaller pore sizes; however, local electrostatic effects caused by the charged MMT surfaces may have also contributed.

SUPPORTING INFORMATION

The Supporting Information contains a comparison of the size distributions for the suspension of sodium MMT (representative AFM images and histograms of the digital image analysis results are given). Additional information presented includes three Kratky plots for the SAXS data showing linear fits for the control, random, and magnetized composite hydrogels.

The authors thank Dazhi Liu for many helpful discussions and user access in performing the SANS analysis at Oak Ridge National Laboratory's Spallation Neutron Source. Magnetic orientation was performed at Oak Ridge National Laboratory's High and Thermal Magnetic Processing facility. Many thanks are owed to Gerry Ludtka for helpful discussions and use of the 9-T superconducting magnet. One of the authors (J.W.T.) gratefully acknowledges being the recipient of a University Diversity Fellowship from Tennessee Technological University. The authors are indebted to the continued support from the Center for Manufacturing Research of Tennessee Technological University and for use of the SAXS instrumentation.

References

1. Ham, M. J.; Kim, Y. H. Polym Eng Sci 2008, 48, 2439.
2. Haraguchi, K.; Takehisa, T. Adv Mater 2002, 14, 1120.

3. Haraguchi, K.; Matusuda, K. Chem Mater 2005, 17, 931.
4. Haraguchi, K.; Farnsworth, R.; Ohbayashi, A.; Takehisa, T. Macromolecules 2003, 36, 5732.
5. Haraguchi, K. Macromol Symp 2007, 256, 120.
6. Haraguchi, K.; Takehisa, T.; Fan, S. Macromolecules 2002, 35, 10162.
7. Zhao, X.; Ding, X.; Deng, Z.; Zheng, Z.; Peng, Y.; Long, X. Macromol Rapid Commun 2005, 26, 1784.
8. Okay, O.; Opperman, W. Macromolecules 2007, 40, 3378.
9. Simhadri, J. J.; Stretz, H. A.; Oyanader, M.; Arce, P. E. Ind Eng Chem Res 2010, 49, 11866.
10. Pennathur, S.; Santiago, J. G. Anal Chem 2005, 77, 6782.
11. Matos, M. A.; White, L. R.; Tilton, R. D. Colloids Surf B 2008, 61, 262.
12. Yu, C.-J.; Su, C.-L.; Tseng, W.-L. Anal Chem 2006, 78, 8004.
13. Thompson, J. W.; Stretz, H. A.; Arce, P. E. Ind Eng Chem Res 2010, 49, 12104.
14. Liang, D.; Song, L.; Chen, Z.; Chu, B. Electrophoresis 2001, 22, 1997.
15. Huang, G.; Zhang, Y.; Ouyang, J.; Baeyens, W. R. G.; Delanghe, J. R. Anal Chim Acta 2006, 557, 137.
16. Fu, J.; Schoch, R. B.; Stevens, A. L.; Tannenbaum, S. R.; Jongyoon, H. Nat Nanotechnol 2007, 2, 121.
17. Koerner, H.; Hampton, E.; Dean, D.; Turgut, Z.; Drummy, L.; Mirau, P.; Vaia, R. Chem Mater 2005, 17, 1990.
18. Ploehn, H. J.; Liu, C. Ind Eng Chem Res 2006, 45, 7025.
19. Tanaka, T.From Gels to Life; University of Tokyo Press: Tokyo, 2002.
20. Fornes, T. D.; Paul, D. P. Polymer 2003, 44, 4993.
21. Hegde, R. R.; Bhat, G. S. J Appl Polym Sci 2010, 118, 3141.
22. Mallia, V. A.; Terech, P.; Weiss, R. J Phys Chem B 2011, 115, 12401.
23. Gonzalez-Meijome, J. M.; Lopez-Alemany, A.; Almeida, J. B.; Parafita, M. A. J Biomed Mater Res Part B: Appl Biomater 2005, 76, 419.
24. Apkarian, R. P.; Wright, E. R. Microsc Microanal 2005, 11, 1088.
25. Gaharwar, A. K.; Dammu, S. A.; Canter, J. M.; Wu, C.-J.; Schmidt, G. Biomacromolecules 2011, 12, 1641.
26. Jain, S.; Dyrdahl, M. H. E.; Gong, X.; Sriven, L. E.; Bates, F. S. Macromolecules 2008, 41, 3305.
27. Taribagil, R. R.; Hillmyer, M. A.; Lodge, T. P. Macromolecules 2010, 43, 5396.
28. Stellwagen, N. C. Electrophoresis 2009, 30, S188.
29. Gemeinhart, R. A.; Park, H.; Park, K. Polym Adv Technol 2000, 11, 617.
30. Stretz, H. A.; Paul, D. R.; Cassidy, P. E. Polymer 2005, 46, 3818.
31. Nie, J.; Du, B.; Oppermann, W. Macromolecules 2005, 38, 5729.
32. Benguigui, L.; Boue, F. Eur Phys J B 1999, 11, 439.
33. Horkay, F.; Burchard, W.; Geissler, E.; Hecht, A.-M. Macromolecules 1993, 26, 1296.
34. Geissler, E.; Horkay, F.; Hecht, A.-M.; Rochas, C. Polymer 1997, 38, 15.
35. Hecht, A.-M.; Geissler, E. Phys Rev E 1999, 59, 1976.
36. Sharma, J.; Aswal, V. K.; Goyal, P. S.; Bohidar, H. B. Macromolecules 2001, 34, 5215.
37. Willcox, P. J.; Howie, D. W.; Schmidt-Rohr, K.; Hoagland, D. A.; Gido, S. P.; Pudjijanto, S.; Kleiner, L. W.; Venkatraman, S. J Polym Sci Part B: Polym Phys 1999, 37, 3438.
38. Koberstein, J. T.; Picot, C.; Benoit, H. Polymer 1985, 26, 673.
39. Shibayama, M. Macromol Chem Phys 1998, 199, 1.
40. Higgins, J. S.; Benoit, H. C.Polymers and Neutron Scattering; Clarendon: Oxford, United Kingdom, 1994.
41. Walldal, C.; Akerman, B. Langmuir 1999, 15, 5237.
42. Ritacco, H.; Albouy, P.-A.; Bhattacharyya, A.; Langevin, D. Phys Chem Chem Phys 2000, 2, 5243.
43. Kulicke, W. M.; Kniewske, R.; Klein, J. Prog Polym Sci 1982, 8, 373.
44. Lape, N. K.; Nuxoll, E. E.; Cussler, E. L. J Membr Sci 2004, 236, 29.
45. Paul, D. P.; Robeson, L. M. Polymer 2008, 49, 3187.
46. Fredrickson, G. H.; Bicerano, J. J Chem Phys 1999, 10, 2182.
47. Bharadwaj, R. K. Macromolecules 2001, 34, 9189.
48. Ruchel, R.; Steere, R. L.; Erbe, E. F. J Chromatogr A 1978, 166, 563.
49. Hecht, A.-M.; Duplessix, R.; Geissler, E. Macromolecules 1985, 18, 2167.
50. Mallam, S.; Horkay, F.; Hecht, A.-M.; Geissler, E. Macromolecules 1989, 22, 3356.
51. Badjic, J. D.; Kostic, N. M. Chem Mater 1999, 11, 3671.
52. Holen, E.; Elsayed, S. Int Arch Allergy Immunol 1990, 91, 136.
53. Yu, C.-J.; Su, C.-L.; Tseng, W.-L. Anal Chem 2006, 78, 8004.